ELSEVIER

Materials Science and Engineering A307 (2001) 158–164

MATERIALS SCIENCE & ENGINEERING A

www.elsevier.com/locate/msea

A high temperature deformation mechanism map for the high performance Ni-base superalloy GTD-111

S.A. Sajjadi *, S. Nategh

Faculty of Materials Science and Engineering, Sharief University of Technology, Azadi Avenue, P.O. Box: 11365-8639, Tehran, Iran

Received 10 December 1999; received in revised form 2 October 2000

Abstract

GTD-111, used for gas turbine first stage blades, is a new, high performance and less investigated Ni-based superalloy. This alloy, with high volume fraction of γ' phase, has excellent creep resistance. It is believed that several creep deformation mechanisms operate at various combinations of temperature and stress. The regions of the controlling mechanisms can be described in terms of a stress-temperature deformation mechanism map. To construct a creep mechanism map for GTD-111 superalloy, single-specimen creep tests at constant stress/variable temperature and constant temperature/variable stress were conducted. The map consists of two separate dislocation controlling mechanism fields; a stacking fault and anti-phase boundary region, and a dislocation climb region. Also, it was clear that a diffusional creep mechanism operated at lower stresses. Microstructural analysis using TEM on creep tested specimens in the two dislocation creep fields confirmed the deformation mechanism map for GTD-111 superalloy.

Keywords: GTD-111; Ni-base superalloy; Creep behavior; Deformation mechanism

1. Introduction

The nickel-base superalloy GTD-111, which was designed in the mid-1970s by the General Electric company, is used as a blade material in the first row high pressure stage of gas turbines. It is reported [1] that this alloy is superior by about 20°C in creep-rupture strength in comparison with another Ni-base superalloy, IN-738LC. IN-738LC has a chemical composition and microstructure similar to that of GTD-111 as indicated in Table 1. In addition, the low-cycle fatigue resistance of GTD-111 is better than that of IN-738LC. Gaudenzi et al. [2] studied coating resistance on several alloys using the Dean test and holding at high temperatures for long periods and showed that hot oxidation and corrosion resistance of GTD-111 is much higher than that of IN-738LC. The alloy contains refractory elements such as Mo, W, Ta, Cr and Co to prevent local hot corrosion [3]. GTD-111 superalloy, in fact, is a modification of Rene 80 and has a multi-phase microstructure consisting fcc γ matrix, bimodal γ' precipitates (primary and secondary), γ–γ' eutectic, carbides and a small amount of deleterious phases such as σ, δ, η and Laves [4].

In spite of the importance of GTD-111 in manufacturing of hot components such as the first stage blades of gas turbines, unfortunately there is limited investigation and data about this high performance superalloy.

The Ni-base superalloy GTD-111 expends almost all of its life in creep deformation. Therefore, it is worth of studying its creep deformation mechanisms at various combinations of stress and temperature. Several papers related to creep in superalloys indicate an increase in the slope of the log ε–log σ at high stresses and a decrease in the slope of the log $\varepsilon - 1/T$ with decreasing temperature [5–9].

This work used single-specimen creep tests and transmission electron microscopy of specimens crept at different conditions to construct a deformation mechanism map for the alloy. Deformation mechanism maps provide a powerful tool to develop high temperature alloys, to achieve more resistant alloys and to rationalize the creep behavior of these alloys. The me-

* Corresponding author. Fax: +98-21-6005717.
E-mail address: sajadi@mtl.sharif.ac.ir (S.A. Sajjadi).

0921-5093/01/$ - see front matter
PII: S0921-5093(00)01822-0

Table 1
Chemical compositions of GTD-111 and IN738LC superalloys

	Ni	Cr	Co	Ti	W	Al	Ta	Mo	Fe	C	B
GTD-111	Bal.	13.5	9.5	4.75	3.8	3.3	2.7	1.53	0.23	0.09	0.01
IN738LC	Bal.	16.0	8.3	3.38	2.6	3.4	1.7	1.70	0.10	0.11	0.01

chanical data and the corresponding microstructures in the superalloy GTD-111 obtained after deformation under various conditions are presented.

2. Experimental procedure

Chemical composition of as received Ni-base superalloy GTD-111 have been determined by means of X-ray fluorescent (XRF), Optical Emission Spectroscopy (OES) and Atomic Absorption. Grain size measurement was performed using Mean Lineal Intercept method. The primary γ' volume percent was determined using SEM, image analyzer and a stereo microscope.

Seven millimeter diameter rods were cut from a standard heat-treated gas turbine blade made from GTD-111 with equiaxed grains between 0.67 and 1.56 mm with an average grain size of 1.2 mm. Test pieces were machined from the rods having 19 ± 0.1 mm gauge length and 3.50 ± 0.01 mm diameter with screw ends according to ASTM E139.

Tensile creep tests were performed using SATEC constant stress machine with a 20:1 lever-arm rig. Temperatures were controlled to ± 1°C and the temperature fluctuations along the gauge length were kept within ± 1°C during the whole experiments. The elongation of the specimen was measured by Linear Variable–Differential Transformer (LVDT) attached to an extensometer. Three creep test procedures were examined.

(1) *Constant temperature/variable stress:* To examine this incremental-loading procedure and to measure the stress exponent, many tests were conducted at six different temperatures from 750 up to 950°C on the alloy.

(2) *Constant stress/variable temperature:* Several incremental temperature tests were carried out at five different stress levels from 250 to 450 MPa to determine activation energy.

In both procedures, tests commenced at a constant temperature (or stress) and at one stress level (or temperature) and when the secondary creep stage is established the stress (or temperature) was increased and the new secondary creep rate determined. This procedure was repeated till entering of the specimen to the third creep stage. At each stress (or temperature), a strain of approximately 0.3–1% occurred before the stress (or temperature) was changed. To obtain more accurate data at least three specimens were examined at each temperature (or stress). Variance in strain rate was less than 17% of the average for the same temperature–stress conditions.

All the above tests were conducted using single-specimen procedures, instead of multiple-specimen procedure. In the microstructural condition of GTD-111 the two procedures are almost equivalent because the superalloy is microstructurally stable under high-temperature creep conditions.

(3) *Constant temperature/constant stress:* This type of creep test was conducted at four conditions, 982°C/152 MPa, 980°C/300 MPa, 800°C/400 MPa, and 760°C/586 MPa to determine the creep mechanism using transmission electron microscopy (TEM) of their creep microstructures, interrupted during steady-state creep.

Disks were cut from the gauge length of the specimens deformed at different conditions normal to the loading axis. They were profiled and thinned using ion milling machine and electrochemical polishing with a double jet polisher using an electrolyte of 7% perchloric acid and 93% acetic acid at -2°C. The foils were then examined at 200 KV in a Philips scanning–transmission electron microscope (STEM). Images are presented in single beam condition.

3. Results and discussion

The chemical composition of the superalloy GTD-111 is presented in Table 1. Study of microstructure of the alloy, at standard heat treated condition, by SEM shows that the structure consists of primary large cube γ' (with edge dimension of 0.8 μm), secondary fine spherical γ' (with 0.1 μm diameter), γ–γ' eutectics and carbides distributed almost uniformly in the γ matrix. The γ' phase is a superlattice possessing the Ll_2-type structure with a nominal composition of Ni_3(Al, Ti). Its long range ordered structure affects glide of dislocations markedly, so, it is well known that γ' is responsible for the strengthening of nickel-base superalloys [10]. In addition, coherency strains, the γ–γ' lattice mismatch, the matrix/particle interface formation energy, anti-phase boundaries (APB) produced during shearing of precipitate by dislocation pairs, and different elastic moduli of the matrix and precipitate contribute to the γ' precipitation hardening in Ni-base superalloy [11,12]. Measurement indicates that this alloy has about 45% primary γ' and 15–20% secondary γ' precipitated in the γ matrix. MC carbides precipitate frequently in the

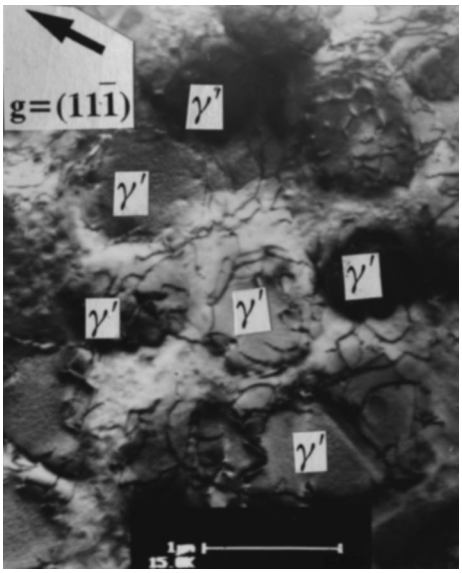

Fig. 1. TEM microstructure of GTD-111 in standard heat treatment condition.

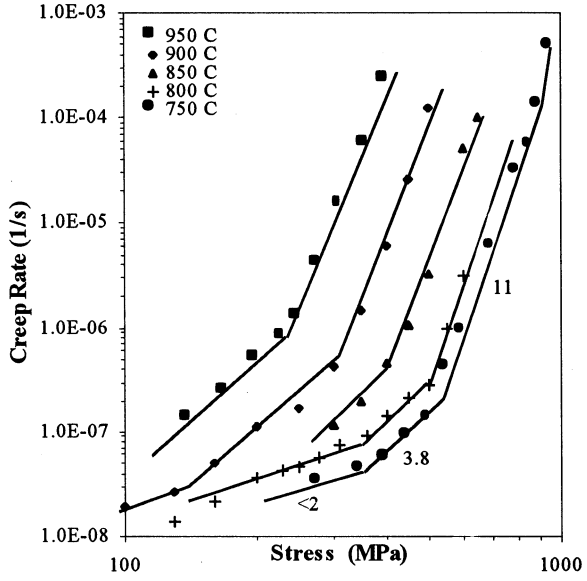

Fig. 2. The stress dependence of the steady state creep rate of GTD-111 at different temperatures. The values represent stress exponent for each creep mechanism.

interior of grains, between dendritic arms, but $M_{23}C_6$ carbides precipitate at grain boundaries. The separate grain boundary-carbides can improve mechanical properties and prevent grain boundary sliding [13]. Fig. 1 indicates TEM microstructure of GTD-111 in standard heat treatment condition showing a low dislocation density in the γ matrix around γ' particles.

Generally, the Ni-base superalloys with complex and multi-phase microstructures are stable at high temperatures and this characteristic is the main reason for using them in critical and severe service conditions. Although there is no report on the microstructure stability of GTD-111, it is expected that the alloy with a high value of γ' and carbides indicates excellent stability at high temperatures. Microstructural study of crept specimens at high temperatures and stresses for a long time showed only a very small shape change in cubic γ' precipitates. Also, the data obtained from variable temperature and stress creep tests, to calculate n and Q values, compare well with those obtained from constant stress and temperature creep tests.

The dependence of the steady-state creep rate, $\dot{\varepsilon}_s$, on stress, σ, and temperature, T, can be described by an equation such as:

$$\dot{\varepsilon}_s = A\sigma^n \exp(-Q_c/RT) \quad (1)$$

in which A and n are constants and Q_c is the activation energy for creep. The values of n and Q_c for GTD-111 as reported for a number of precipitation hardened superalloys [7–9,11,12] depend on both temperature and stress.

Figs. 2 and 3 show the variation of the secondary creep rate with stress and temperature, respectively. The data obtained at each temperature appear to lie on two or three straight lines, with different slopes. Fig. 2 shows three different n-values for GTD-111 over wide ranges of temperatures and stresses, calculated from the slopes. Therefore three regions, represented by S (shear), C (climb) and D (diffusion), are distinguished. The higher value (11) is associated with shear mechanism including stacking fault and anti-phase boundary formation. $n = 3.8$ is associated with dislocation climb, and the other ($n < 2$) is stress exponent for diffusional creep. These n-values obtained for GTD-111 are consistent with the values reported by other investigators for a number of superalloys [7,14–20]. With increasing temperature the transition from dislocation to diffu-

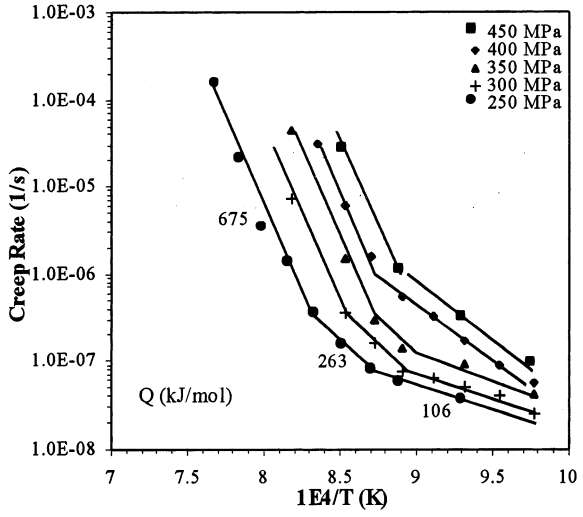

Fig. 3. The temperature dependence of the steady state creep rate of GTD-111 at different stresses. The values represent activation energy for each creep mechanism.

sional creep occurs at lower stresses. Also, above about 900 MPa the deformation mechanism changes. This mechanism as proposed by Carey et al. [21] for IN-738LC and Frost and Ashby [22] for MAR-M200, may be obstacle controlled dislocation glide.

Fig. 3 is plotted using the results obtained from the variable–temperature creep tests at constant stress. In order to determine the apparent activation energy for creep, an Arrhenius type relationship (Eq. (1)) was assumed between the steady state creep rate and temperature. Using this relationship three values of 675, 263 and 106 kJ/mol were obtained, similar to other observations for precipitation hardened superalloys [7,14–20,23].

The different creep activation energies define three creep mechanisms operating over wide ranges of temperature and stress, as indicated before. The two larger activation energies, frequently reported for multi-phase superalloys, have been associated with creep controlled by dislocation motion. When stress is sufficiently high and precipitate and matrix have the same crystal structures and orientations, as in GTD-111, the matrix dislocations can shear the particles. When dislocation climb is controlling process, the activation energy is equal to the self-diffusion activation energy. It has been reported [24] that the self-diffusion activation energy for Ni-based superalloys is in the range 257–283 kJ/mol and for GTD-111 is 259 kJ/mol, is in good agreement for region C. The region with the small slope (activation energy) is related to diffusional creep.

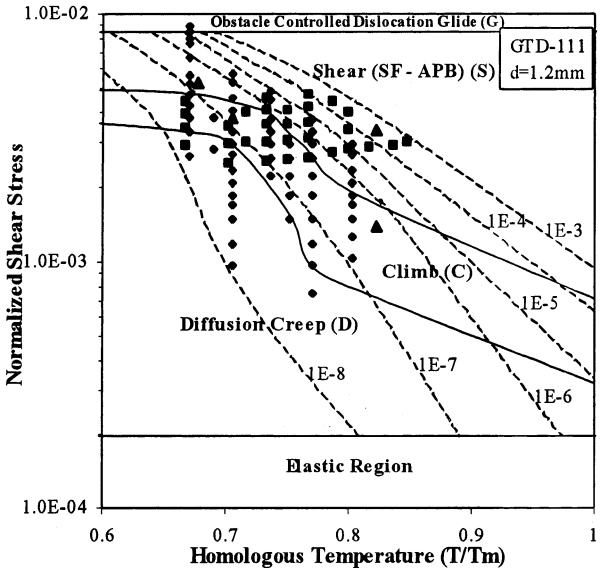

Fig. 4. A deformation mechanism map for GTD-111 with an average grain size of 1.2 mm. $T_m = 1523$°K. Contours represent creep rate in per s. ◆, the data obtained from constant temperature/variable stress. ■, the data obtained from constant stress/variable temperature. ^, The data obtained from constant temperature/constant stress used for TEM study.

With combination of the two sets of data, the deformation mechanism map shown in Fig. 4 is constructed. Deformation mechanism maps are a useful means of determining the creep mechanism operating in a definite region of the map. In the construction of the map the incipient melting temperature, T_m, is considered 1523°K and the applied stress is converted to the equivalent shear stress normalized by the shear modulus at each temperature [22].

The high temperature deformation mechanism map indicates a high-stress plasticity region controlled by dislocation glide, two power-law creep regions and a grain boundary diffusion creep region at low stresses. The diffusional creep region (represented as D) has activation energy of 106 kJ/mol, which is nearly the same value obtained for MAR-M200 by Frost and Ashby [22]. A transition from boundary (Coble) to lattice (Nabarro-Herring) creep mechanism would be expected with increasing temperature in tests undertaken at lower stresses.

The normalized threshold stress for diffusional creep (σ_t/μ) was estimated 2×10^{-4} using the following equation [21]:

$$\sigma_t/\mu \sim b_b/L \quad (2)$$

in which L is the spacing of obstacles (γ' precipitates) in grain boundaries and b_b is Burgers vector for grain boundary dislocations ($\sim 8.33 \times 10^{-11}$ m). Substituting the data reported for IN-738LC [21], which are approximately the same as those of GTD-111, in the above equation, the value of $\sim 2 \times 10^{-4}$ is obtained and indicated in Fig. 4.

The results of study on creep tested specimens interrupted during stage II using TEM show that at high stresses, when $n \sim 11$, dislocations cut through γ' particles by stacking fault (SF) formation and anti-phase boundary (APB) coupled dislocation pairs. The creep induced dense dislocation networks are mainly constrained at the γ–γ' interface. Fig. 5 shows the TEM microstructure of the specimen creep tested in the dislocation creep region S. Since the intrinsic stacking faults are lying on a common (111) glide plane [25], the matrix dislocations must, as totals, dissociate into partials at the γ–γ' interface, producing a single superpartial gliding in the γ' phase and a partial left at the interface which relaxes the high coherency stresses at γ–γ' interfaces. Therefore, the partial reduces the overall energy of the dislocation interface configuration so that a stacking fault formation can be generated at a coherent interface. After passing the precipitate, the partial dislocations rearrange themselves to totals for further motion in the matrix. Groups of partial dislocations may create a variety of fault configurations in γ' precipitates. Various types of fault configurations were observed in specimen creep tested under S condition.

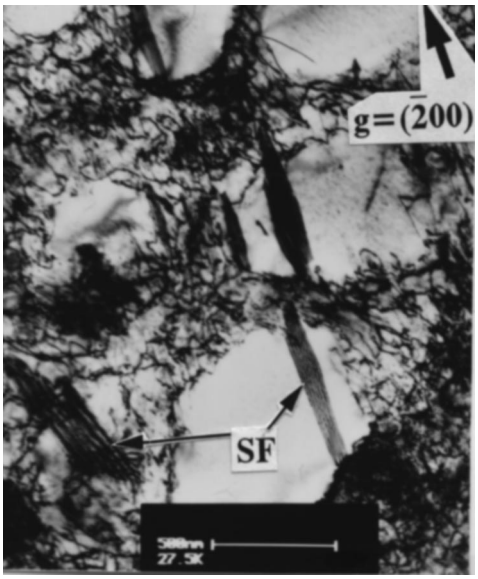

Fig. 5. TEM microstructure showing SF in γ' precipitates in the specimen creep tested at 760°C/586 MPa in the dislocation creep region S and interrupted at steady state creep stage. With 2.27% strain and $\dot{\varepsilon}_s = 7.12 \times 10^{-7}\,s^{-1}$.

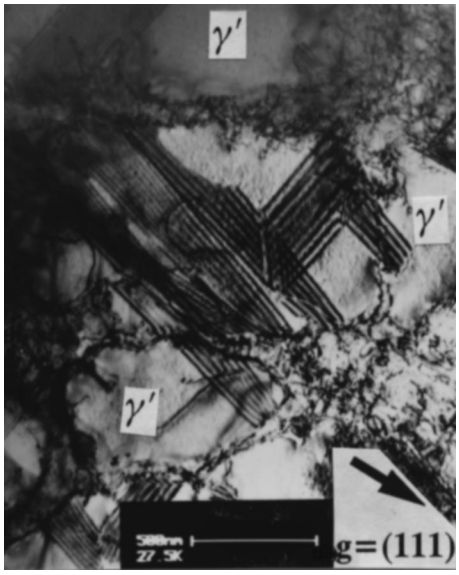

Fig. 6. Stacking fault locks created during creep at 760°C/586 MPa in the dislocation creep region S and interrupted at steady state creep stage. With 2.71% strain and $\dot{\varepsilon}_s = 6.83 \times 10^{-7}\,s^{-1}$.

Kear et al. [26] have proposed coherent interfaces as requirements for stacking fault formation. Otherwise, the resulting pileups of matrix dislocations at the interfaces generate local stresses and cause a transition from stacking fault to APB mechanism.

Observation of the microstructure of GTD-111 at the end of stage II indicates high densities of stacking faults in γ' precipitates and increasing the probability of stacking fault interactions. An example of the microstructure is shown in Fig. 6 where reactions of stacking faults from different {111} planes have created locks. Also at this high creep strain and high stress in addition to stacking faults, a few pairs of $a/2\langle 110\rangle$ screw dislocations are observed on {111} glide planes inside γ' cubes (Fig. 7). The paired dislocations, well separated in the matrix, are constricted upon entering the γ' particle due to the creation of the APB between them. Sometimes this constriction is so high that the dislocation pairs, which are resolvable in the matrix, are not observed in the γ' precipitates [9]. From an energetic point of view, the shear mechanism by APB-coupled dislocation pairs occurs when matrix dislocations pileup at the interfaces in order to push the leading dislocation into the γ' cubes, as has been described by Link and Feller-Kniepmeier [25]. Therefore, this mechanism, predominant at high stresses and high strains, is not likely to occur at low strains with insufficient dislocation densities for pileups at the interfaces. So, it is expected that in the upper range of this region (S) APB-coupled dislocation pair is the dominant mechanism and in the lower range the SF formation is predominant [9].

At low stresses, when $n \sim 4$, the dislocations are unable to cut through or bow between the particles. Deformation is based now on the movement of dislocations in the matrix and the change of the γ' morphology [27]. In this region it has been suggested either the dislocations are forced to overcome the particles by climb [28], or alternatively, deformation occurs predominantly in the grain boundary zones, i.e. by grain boundary sliding and deformation in regions of the grains adjacent to the boundaries [29,30]. The disloca-

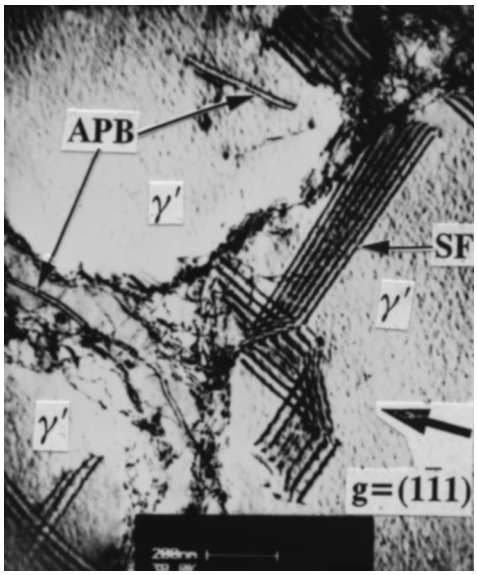

Fig. 7. TEM microstructure showing SF and APB-type shearing mechanism in the specimen creep tested at 760°C/586 MPa in the dislocation creep region S and interrupted at steady state creep stage. With 2.71% strain and $\varepsilon_s = 6.83 \times 10^{-7}\,s^{-1}$.

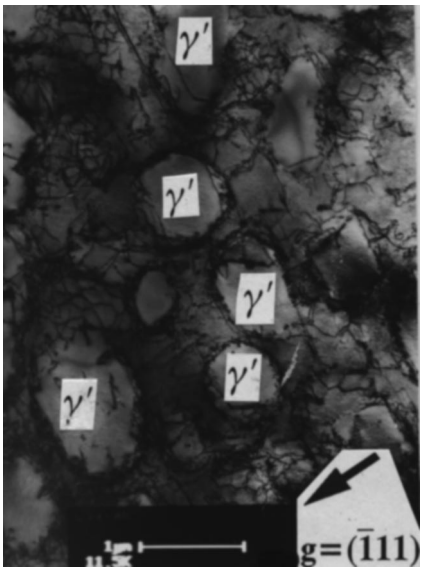

Fig. 8. TEM microstructure showing the dislocation configurations in the specimen creep tested at 982°C/152 MPa in the dislocation climb region C and Interrupted at steady state creep stage. With 2.43% strain and $\varepsilon_s = 3.80 \times 10^{-7}\,s^{-1}$.

tion configurations in the grains, which are the representative of dislocation climb process, are illustrated in Fig. 8 for GTD-111 specimens creep tested in region C. It is clearly shown that dislocations migrate mainly within γ matrix in creep processes and many dislocation networks, after climbing over γ' particles, exist at γ–γ' interfaces. No evidence has been observed showing dislocations cut through γ' particles. This figure also shows homogeneous distribution of low-density dislocations within matrix phase, network formation at the γ–γ' interfaces with little or no dislocations in the γ' particles.

The boundaries between S and C regions and between C and D regions appear to be independent of temperature up to about 800°C. These results are in good agreement with earlier investigations on IN738LC alloy with two γ' morphologies [9,11,12].

4. Conclusions

From the study of creep behavior of the cast nickel base superalloy GTD-111 the variation of the steady-state creep rate with stress and temperature could be expressed as an Arrhenius type relationship.

The creep behavior is in agreement with the behavior of precipitation strengthened alloys which on decreasing stress show a transition from more stress-sensitive cutting of γ' precipitates to less stress-sensitive climb and diffusion. The deformation mechanism map constructed by the data obtained from creep tests at variable stress and temperature predicts the creep mechanism operating in a definite region of the map. Three different mechanisms of interaction between dislocations and γ' precipitates in GTD-111 have been microscopically observed. The occurrence of a given mechanism depends on the test conditions of temperature and stress. A shear mechanism involving stacking fault and anti-phase boundary coupled dislocation pair formation in the γ' precipitates occurs over a wide range of experimental conditions. Dislocation climb over γ' precipitates and diffusional creep through grain boundaries are the other mechanisms operating at lower stresses.

Acknowledgements

The authors wish to express appreciation to Mavadkaran Eng. Co. for supporting of this project. Also, Tavanir, Deputy of Research and Technology, is gratefully acknowledged for providing the material.

References

[1] P.W. Schilke, A.D. Foster, J.J. Pepe, A.M. Beltran, Advanced materials and processes 4 (1992) 22–30.
[2] G.P. Gaudenzi, A. Colombo, G. Rocchini, F. Uberti, Presented at conf.: Elevated Temp. Coatings, Sci. and Tech. II, California, USA, 4–8 Feb. 1996, 301–310.
[3] General Electric Co., M-715, 1–18, 1980.
[4] G.K. Bouse, Presented at conf.: Superalloys 1996, Champion, Pennsylvania, 22–26 Sept. 1996, 163–172.
[5] A.C. Picasso, A.J. Marzocca, I. Alvarez, Materials Sci. Eng. A234–236 (1997) 1099–1102.
[6] W. Blum, in: H. Mughrabi (Ed.), Materials Sci. and Tech, vol. 6, VCH, New York, 1993, p. 359.
[7] V. Lupinc, in: R. Brunetaud, et al. (Eds.), High Temp. Alloys for Gas Turbine, Reidel Publishing Co, 1982, pp. 395–419.
[8] A.K. Koul, R. Bruntaud, Proceedings of ASM 1993 Materials Congress, Pittsburgh, Pennsylvania, Oct. 17–21 1993, 75–88.
[9] D. Mukherji, F. Jiao, W. Chen, R.P. Wahi, Acta Metall. Mater 39 (7) (1991) 1515–1524.
[10] D.P. Pope, S.S. Ezz, Int. Metals Rev. 29 (3) (1984) 136–167.
[11] P.J. Henderson, M. McLean, Acta Met. 31 (8) (1993) 1203–1219.
[12] R.A. Stevens, P.E.J. Flewitt, Acta Met. 29 (1981) 867–882.
[13] C.R. Brooks, Heat treatment, structure and properties of non-ferrous alloys, ASM, 1982 (Chapter 5).
[14] J.P. Dennison, P.D. Holmes, B. Wilshire, Materials. Sci. and Eng. 33 (1978) 35–47.
[15] G.F. Harrison, W.J. Evans, In: Proc. Conf. 'Eng. Aspects of Creep', The Inst. Mech. Engineers, Uni. of Sheffield, UK, 1980, 69.
[16] F. Gabrielli, V. Lupinc, Proc. 8th Congr. Mat. Testing, Budapest, 1982.
[17] T.B. Gibbons, S. Osgerby, F. Gabrielli, V. Lupinc, in: R. Brunetaud, et al. (Eds.), High Temp. Alloys for Gas Turbine, Reidel Publishing Co, 1982.
[18] G. Janting, D. Ranucci, E. Picco, P.M. Strocchi, in: R. Brunetaud, et al. (Eds.), High Temp. Alloys for Gas Turbine, Reidel Publishing Co, 1982.
[19] K.R. Williams, B. Wilshire, Met. Sci. J. 7 (1973) 176.
[20] F. Gabrielli, V. Lupinc, Proc. ICSMA 6, Melbourne, 1982.

[21] J.A. Carey, P.M. Sargent, D.R.H. Jones, J. Mater. Sci. Lett. 9 (1990) 572–575.
[22] H.J. Frost, M.F. Ashby, Deformation Mechanism Maps, Pergamon Press, Elmsford, NY, 1982.
[23] Z. Yang, Y. Xiao, C. Shih, Z. Metallkde, 78 (1987) 339–343.
[24] J.A. Daleo, J.R. Wilon, Presented at the International Gas Turbine and Aeroengine Congress and Exhibition, Birmingham, UK, June 10–13, 1996.
[25] T. Link, M. Feller-Kniepmeier, Met. Trans. 23A (1992) 99–105.
[26] B.H. Kear, J.M. Oblak, A.F. Giamei, Metall. Trans. 1 (1970) 2477–2486.
[27] M. Feller-Kniepmeier, T. Link, Met. Trans. 20A (1989) 1233–1238.
[28] G.S. Ansell, J. Weertman, Trans. Metall. Soc. AIME 215 (1959) 838.
[29] P.L. Threadgill, B. Wilshire, Met. Sci. J. 8 (1974) 117.
[30] J.D. Parker, B. Wilshire, Mater. Sci. Eng. 29 (1977) 219.